2021 IEEE/RSJ International Conference on Intelligent Robots and Systems (IROS)
September 27 - October 1, 2021. Prague, Czech Republic

2021 IEEE/RSJ International Conference on Intelligent Robots and Systems (IROS) | 978-1-6654-1714-3/21/$31.00 ©2021 IEEE | DOI: 10.1109/IROS51168.2021.9636324

A Powered Prosthetic Ankle Designed for Task Variability – A Concept Validation

Sameer Upadhye[1*], Chinmay Shah[1], Ming Liu[2], *Member, IEEE*, Gregory Buckner[1] and He (Helen) Huang[2], *Senior Member, IEEE*

***Abstract*— Ankle joints play key roles in everyday locomotion, such as walking, stair climbing, and sit-to-stand. Despite the achievement in designing powered prosthetic ankles, engineers still face challenges to duplicate the full mechanics of ankle joints, including high torque, large range of motion (ROM), low profile, backdrivability, and efficiency, using electric motors and related transmissions. In this study, our goal was to develop a new active prosthetic ankle, *Variable Spring embedded Motor-ball screw (VSeM)* ankle, to meet all these requirements at the same time. Using a manually adjustable elastic element, which is parallel with our motor actuator, we can readjust the ROM of *VSeM* to handle all normal locomotion tasks. *VSeM's* capability to mimic human ankle was validated through both bench tests and human subject tests.**

I. Introduction

A. Motivation

Major lower-limb amputations negatively impact the quality of life of over 600,000 people living in the United States; the associated loss of mobility creates hurdles for healthy independent living [1-4]. Hence, the development of high torque, low weight, and efficient ankle prosthetic devices are essential for improving the quality of life for lower-limb amputees. However, the development of a powered prosthesis still faces significant engineering challenges.

Besides providing the needed torque during normal level-ground walking, a powered prosthetic ankle with clinical merits must be 1) self-contained with a lower profile, which is comparable to a normal ankle joint; 2) maintain a reasonable range of motion (ROM) to conduct various tasks; 3) backdrivable to ensure user comfort [5], and 4) high efficiency to prolong its walking range (no. of steps after each battery recharge). It is a real practical challenge to meet all these requirements at the same time.

Engineers usually adopt two types of design to meet these requirements: active driven (AD) and active driven with parallel elastic elements (ADPEE). The AD solution purely relies on active actuators. Because current actuator technologies, usually electrical motors with transmissions, lacks the requisite torque and power densities of their natural counterparts [6-8], engineers adopt innovative transmission systems, which can generate large transmission ratio with the sacrifice of range of motion (ROM) [9], back-drivability[10], or carry a relatively high profile [11]. Because all the power is from the active motor, energy consumption is expected to be high, although some energy harvesting functions are often embedded in the power module of these prostheses. Engineers often are forced to rely on overcurrent, which is very energy inefficient, to generate the needed short-term torque burst.

ADPEE is also a very common design approach in powered prosthetic ankles [6,7,13-14]. If designed correctly, the passive elements release stored energy when high torque/power is needed, so the prosthetic ankle can meet the torque/power requirement with smaller active actuators, which also leads to a reduction of the ankle profile. The energy efficiency is also improved due to the low torque requirement and high efficiency of the passive elements.

Adopting ADPEE brings additional design challenges. The performance of the passive elements depends on their stiffness and equilibrium positions. To reduce the size of the passive elements and its supporting structure, designers generally prefer a high stiffness spring, which can meet the torque requirement with small deformation and permit the equilibrium to be set close to where the maximum torque is needed. However, a spring with a fixed equilibrium position and high stiffness can effectively limit ROM when the ankle moves in the direction opposite to which the maximum torque is needed. Because the peak torque usually occurs along plantarflexion, limited dorsiflexion is a common feature for these powered prosthetic ankles and is regarded as a needed compromise to ensure high torque and low profile at the cost of task variability. This limitation could not be mitigated by adjusting controllers. Table I. compares various aspects of different AD and ADPEE ankle prostheses.

Although normal walking with a ROM -0.25 rad ~ 0.35 rad (dorsiflexion is positive) only involves limited dorsiflexion [15], the capability to conduct dorsiflexion is very important for tasks, such as stair walking [16], sitting to standing [17], and squatting [18]. Limited dorsiflexion leads to additional compensation efforts and poor user experience.

Changing the dynamical properties of the elastic elements is one of the solutions to expand the dorsiflexion in ADPEE systems. Some semi-active prosthetic ankles have been designed to realize adjustable properties of the elastic elements, by using electrically modulated spring mechanisms [19-20]. Such systems typically lack an active power element due to weight considerations; they only

[1]Research was partially supported by the National Science Foundation through award 1808898.

*Sameer Upadhye (supadhy2@ncsu.edu) is the corresponding author.
[1]Department of Mechanical and Aerospace Engineering, North Carolina State University, Raleigh, NC, 27695, USA
[2]Joint Department of Biomedical Engineering, North Carolina State University/University of North Carolina Chapel Hill, NC, USA

Table I. COMPARISON OF VARIOUS AD/ADPEE ANKLE PROSTHESES.

Device	*Passive Element*	*ROM (DF-PF) (radians)*	*Mass (kg)*	*Height (cm)*	*Peak Torque (Nm)*
BioM [8]	Series and Parallel	0.174-0.42	2.2	19	125
OSL [9]	None	0.52 (Total)	1.74	21.3	140
VU Leg 3 [11]	Parallel	0.52-0.78	2.3	30	140
p^2 ankle [12]	None	0.49-0.47	1.0*	12	125
Tf-8 [21]	Series	0.36-0.69	1.6*	24.4	175
VSeM (NCSU)	Parallel	0.52-0.44	1.9*	21	138

*without batteries or electronics

change the stiffness of the elastic elements, which does not increase the ROM significantly.

In this work, we developed the *VSeM Ankle (**V**ariable **S**pring **em**bedded **M**otor-ball screw **Ankle**)*, a powered prosthetic ankle, which has adjustable components to achieve the different biological kinetics and kinematics, using ADPEE. Designed as a platform to study the ankle performance under various tasks, the device was optimized for maximizing torque with permitted profile, so we could systematically evaluate the impacts caused by changing the properties of the elastic elements. Compared with existing external powered prosthesis simulators, such as [18,22-23], this platform permits amputees to move freely if a battery is used as the power source.

Two major innovations of this design include: 1) a spring mechanism, which features high offline stiffness and equilibrium angle manipulability, achieved via a slider-crank mechanism incorporating Belleville springs. The desired variation in the properties of the elastic elements can be easily achieved by manually altering the spring stack configuration; and 2) a screw-embedded actuator design, which achieves a significant size reduction in actuator length and obviates the need for repeated maintenance, which is often needed when timing belts are involved [24]. This system was preliminarily validated through both bench tests and human subject tests.

II. Methods

A. Design requirements and desired outcomes

The device was designed for a human weight of 75 kg (ankle torque of 120 Nm for walking), the minimum desired range of motion (ROM) of 0.87 rad, and maximum height and mass specifications of 23.0 cm and 2.5 kg, respectively. These criteria were selected based on the specifications for commercially available prostheses and average human ankle-shank weight [6].

B. Design and fabrication of actuation mechanism

The active ankle design, shown in Fig. 1, utilizes a four-bar linkage mechanism for higher torque density [9]. This actuator consists of an embedded motor ***C***, fixed to the support frame by revolute joint ***D***. This motor drives a ball screw, with a ball nut hinge connected at ***B*** to the foot-crank. The foot-crank complex (crank fixed to the prosthetic foot) forms a revolute joint at ankle joint ***A*** with the support frame and clevis. Hence, as the motor rotates the ball screw, the distance between the ***B*** and ***D*** changes, causing rotation

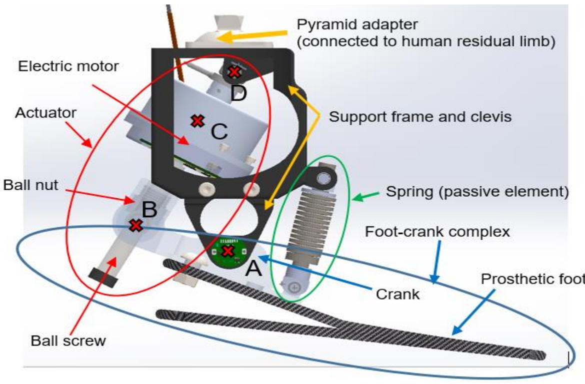

Figure 1. Side view of the actuated prosthetic ankle prototype, showing linkage components with the motorized actuator (red), prosthetic foot-crank complex (blue), and spring (green). Joints A, B, C, and D represent the ankle joint, crank-actuator revolute joint, stator-rotor rotary joint (with rotation about the actuator's length axis), and motorized actuator-support frame revolute joint, respectively (located by crosses). The support structures are indicated by yellow arrows.

of the foot-crank about the ankle joint (***A***). Compared with traditional motor-connector-ball screw design and timing belt-driven ball screw designs [6-8], the ball-screw-embedded actuator can reduce the total size of the actuator and reduce maintenance challenges.

A frameless motor kit (Celera Motion model UTH-63-B-18-C-x-000, rated torque: 0.268 Nm) and a ball screw with 2mm pitch (SKF model SD 12x2R 82_125_G7_L-Z_WPR) were selected based on force, velocity, and mounting considerations. A brief description of the motor construction (shown in Fig. 2) was provided below. The stator housing and lower shell (with the mounted encoder chip) are fastened together, while the stator (with the Hall sensing board) was glued to the stator housing via epoxy adhesive, all together to form the 'stator system'. The rotor (with the embedded ball screw and connector), the encoder ring, and the encoder mount formed a 'rotor system' sub-assembly, as shown in Fig. 2. The 'stator and rotor systems' were connected structurally via two face-to-face angular contact bearings, forming a rotational joint (referred to previously as 'C'). Finally, a Futek inline load cell (Futek Model FSH03905) was selected for its load capacity and external torque holding capacity and was embedded on the stator housing to measure the force along the actuator length. A custom adapter ('motor pin') was manufactured from AISI 4140 (for higher strength) to align the load cell along the axis of the actuator and mount the entire subassembly on the support frame.

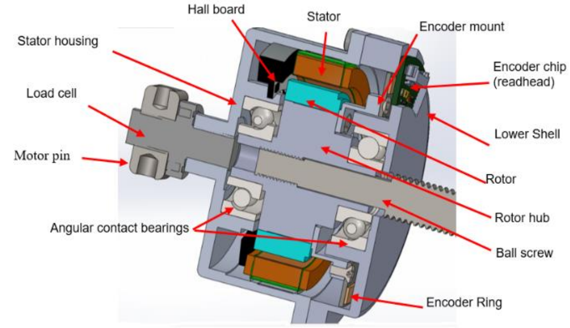

Figure 2. The cross-sectional view of the actuator with the principal internal components shown.

C. Design of passive element

Belleville (disc) springs in a slider-crank mechanism were employed, as shown in Fig. 3. Belleville springs have a significant advantage in stack configuration versatility. This process does not require the change of the entire passive element and essentially the change can be achieved by swapping different stiffness Belleville springs and/or adding hardened washers (for stack height adjustment). This enables easy offline modulation of passive element angular stiffness and equilibrium angle. A quick simulation using two different belleville springs (with individual stiffnesses K1=2578 N/mm and K2=6684 N/mm but with same ID and OD for use in the same element) showed that for the same stack height (within RMS error of 1.69% and peak error of 3.98%), the effective angular stiffness of the passive element (at ankle) could be varied from 200 to 550 Nm/rad by increments of 10 Nm/rad with RMS error of 2.38% and peak error of 7.00% by means of simply varying stack configuration using the two springs in series. Hence, with more potential combinations, the passive element's resolution can be very high. This mechanism involves a series spring stack mounted on a steel piston rod (A2 Steel, HRC 38), with the rod forming a prismatic joint at the upper spring mounting bracket (7075-T7351 grade aluminum). The upper spring mounting bracket forms a revolute joint at the two hinges on the support frame as shown. The other end of the piston rod is threaded to the lower spring mounting bracket (7075-T7351 grade aluminum) which is connected using a pin to the crank, to form a revolute joint.

A hardened steel lock-washer (with HRC 51) is located at the stack end near the upper spring mounting bracket to protect the bracket from damage due to indentation by the springs. Kinematic modeling of the spring mechanism was conducted to study spring engagement during the Controlled Dorsiflexion (CD) and Powered Plantarflexion(PP) phases for ankle angles greater than the set equilibrium angle (θ_o).

One spring configuration cannot satisfy the requirements for all locomotion conditions. This can be observed by studying the effect of the different passive element stack configurations on the required actuator torque (at the ankle). This can be readily computed using able-bodied data on ankle torque-angle characteristics. Fig. 4(a) and (b) showed the required torque needed by the active actuator for stair ascent and level ground walking with different stack configurations of the elastic element. As shown in Fig.4(a), the required torque for k_{spring} = 100 Nm/rad and θ_o = -0.20 rad was within the actuator's rated torque limits. The configuration with k_{spring} = 342Nm/rad and θ_o = -0.07 rad

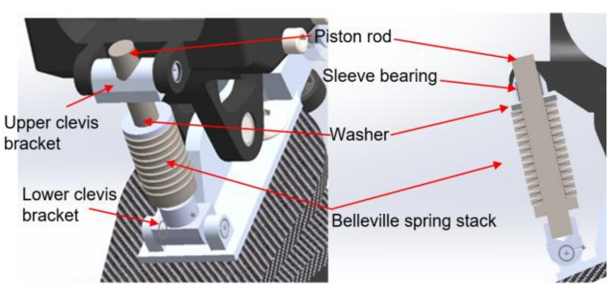

Figure 3. Frontal (left) and side section (right) views of the spring element (differing spring configurations are shown to clarify modular functionality)

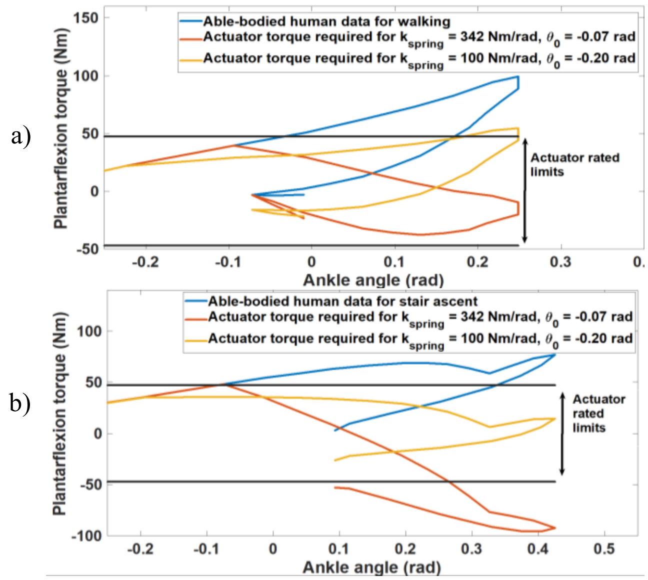

Figure 4. Comparison of (a) stair ascent and (b) walking, ankle torque-angle curves for able-bodied individual [19] and required actuator torque for two different stack configurations of the passive element where k_{spring} = 342 Nm/rad at θ_o = -0.07 rad. and k_{spring} = 100 Nm/rad at θ_o = -0.20 rad.

would not be able to generate the needed torque because it requires the actuator to generate 100 Nm, which is beyond the rated actuator torque(47.2Nm) However, in Figure 4(b), when lower dorsiflexion is needed, k_{spring} = 100 Nm/rad and θ_o = -0.20 rad fell out of the torque range permitted by the actuator and the elastic element configuration corresponding to k_{spring} = 342Nm/rad and θ_o = -0.07rad permitted the powered prosthetic ankle to meet the requirement of the torque and ROM at the same time.

D. Structural design and final assembly

Fig. 1 showed the structural parts of the optimized structural design. The support frame , clevis and crank were manufactured from aluminum (grade 7075) for superior strength and weight while the manufacturing was conducted via wire electric discharge machining (EDM) and milling operations. Finite element analysis and topological optimization tools in ANSYS Workbench (Ansys Inc, Canonsburg PA) were used for the optimal design of these three parts. An overall factor of safety of 3 was assumed while designing the device to ensure it is capable of sustaining the required loading during human locomotion. The carbon-fiber prosthetic foot from Ossur (LP-Variflex foot) was selected based on its superior energy and shock absorption characteristics. The crank and support clevis are mounted together at the ankle, forming a revolute joint (***A***) via a steel pin. The spring stack and a connector edge provide the requisite hard stops.

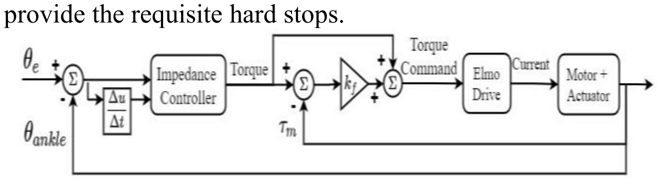

Figure 5. Block diagram for Impedance Control and force feedback. θ_e is the equilibrium angle, θ_{ankle} is the angle measured form the motor encoder and τ_m is the torque measured form the load cell.

E. Control Implementation

An impedance control strategy [6,14] was used for controlling the ankle prosthesis. Fig. 5 depicts the lower-level impedance control and internal force feedback[25]for efficient torque tracking and improving backdrivability.

The real-time control system was implemented using the TwinCAT3–Simulink RT interface on a Windows 10 OS Desktop via an EtherCAT (Ethernet for Control and Automation Technology) protocol. For this study, the TwinCAT 3-Simulink RT-based controller was operated at a sampling rate of 1 kHz. Fig. 6. depicts the flow of connections. Here the BLDC motor was controlled using an Elmo Gold Solo Twitter servo drive (Elmo Motion Control Model G-SOLTWIR50/100EE1S) via the current control mode. This motor has an embedded 18-bit multi-turn absolute BISS-C digital encoder (RLS model MB064DCC18MDDA00) which, along with the stator-embedded Hall effect sensors, is connected to the servo drive. The motor encoder is used to compute the ankle angle via kinematic transformation.

A strain gauge load cell was implemented in-line with the actuator (for reduction of apparent inherent impedance i.e., frictional, and inertial dynamics of the actuator). Two pre-wired strain gauges (OMEGA model KFH-3-120-D16-11L1M2S) are mounted between the heel section and crank mount sections of the prosthetic foot in a half-bridge resistive circuit. The load cell uses a Tacuna Systems amplifier (model EMBSGB200-M), the output of which was connected to the Beckhoff differential four input analog terminal (model EL3104). This terminal is connected via a Beckhoff EtherCAT coupler (model EK1100) to the servo drive using an RJ45 Ethernet Cable. Finally, the servo drive is connected to the desktop computer using an RJ45 Ethernet Cable. The EtherCAT coupler and Elmo Gold Twitter are powered by a 24 V, 20 A power source, while the load cell amplifiers are powered using standard 9V PP3 batteries.

A higher-level finite state control scheme was implemented to perform level ground walking[8] and stair

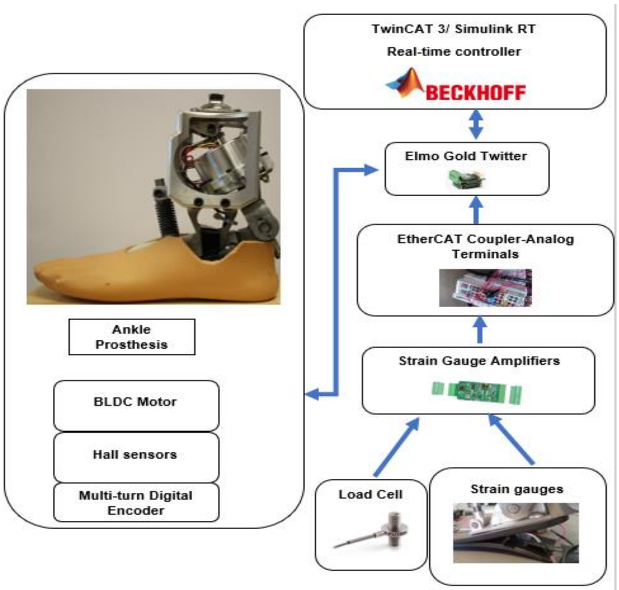

Figure 6. Connection flow chart for the fabricated ankle prosthesis.

ascent tasks[26]. Strain gauge, load cell, ankle angular velocity and ankle angle were used to formulate robust transition rules between the various phases of these tasks.

F. Setups for Ankle Prosthesis test

To quantify the mechanics of our design, the ankle device was mounted on an Instron 4400R universal testing machine (UTM). The carbon fiber foot was removed due to space considerations and the required parts were machined for mounting on the UTM. The setup forms a 4-bar linkage with the ankle point (fixed to the lower jaw) acting as a slider (vertically) while the upper jaw and crank act as two pivoted movable links. Relevant standard angle and load sensors to conduct the tests. The UTM setup provided a triangle wave position input, acting as the external load for both passive element and powered actuator tests.

To validate the potential of this ankle in supporting human locomotion, approved by the IRB at UNC-Chapel Hill, one able-bodied subject (height and weight of 175cm and 75 kg), was recruited to demonstrate the feasibility of the powered prosthesis to support locomotion tasks using a custom bypass orthosis, as shown in Fig.7(b), through treadmill walking (walking speed of 0.8m/s) and the stair ascent case. To measure the kinematics and kinetics of the subject, reflective markers were attached on the subject with Vicon providing the lower body model (plugin gait lower body ai[27]), and a 12-camera based optical motion capture system (MX40+, Vicon, UK) was used to monitor the locomotion at 100Hz. The ground reaction force was measured by force plates, which were embedded in the instrumented treadmill (Bertec, USA), at 1000 Hz. The ankle joint trajectories and ankle joint torques were processed using Visual 3D (C-Motion, Inc., USA). The stair ascent case was studied for two different stack configurations, k_{spring} = 403 Nm/rad at θ_o = 0.00 rad and k_{spring} = 227 Nm/rad at θ_o = 0.10 rad. The spring stiffness combinations and impedance parameters were chosen corresponding to the weight of the participant and tuned to user comfort. The ankle joint trajectories were measured from the motor encoder built into the system.

III. Results

A. Impedance Control and Backdrivability assessment

To validate impedance control, two biomechanically relevant impedance values were selected (based on the able-bodied torque-angle curves and present spring stiffness). The parameters were k_{PP} = 162.4 Nm/rad for ankle angles from -0.30 to -0.03 (derived from powered plantarflexion) and k_{CD} = 179.2 Nm/rad for ankle angles from -0.125 to 0.00 (derived from controlled dorsiflexion). Feedback gain k_f = 2 was used. Figure 8 shows the torque tracking for the impedance control parameters. The mean and peak error values were found to be 2.48 Nm and 6.20 Nm for k_{PP} = 162.4 Nm/rad and 1.63 Nm, respectively, and 3.91 Nm for k_{CD} = 179.2 Nm/rad.

Backdrivability was quantified when an external torque was acted on the ankle and the command torque (shown in Fig. 5) was set to zero. Fig. 9 shows the relationship between the external torque (back-drive torque) and ankle angular velocity when different k_f was adopted. The resulting peak back driving ankle torques were 7.61 Nm for k_f = 0 (no

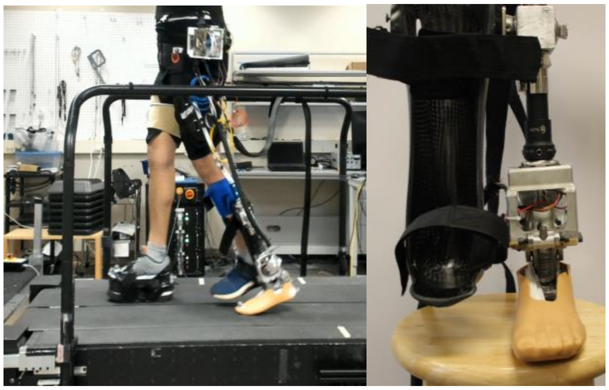

Figure 7. (a) Walking trials with ankle prosthesis on treadmill (b) Ankle prosthesis and the bypass orthosis.

feedback) and 2.04 Nm for $k_f = 3$, respectively. The results confirmed the desired ankle backdrivability.

B. Treadmill Walking and Stair Ascent trials

Fig. 10(a) and (b) compare ankle angle trajectory and ankle torque data collected for the intact side, the *VSeM* prosthesis with that of an able-bodied individual [28,29] while walking on a treadmill at a speed of 0.8m/s.

Fig. 11 compares the stair ascent ankle angle trajectories for two stack configurations of the passive element on the prosthetic ankle with able-bodied individual curves[30]. The two configurations were selected to be $k_{spring} =$ 227 Nm/rad, $\theta_o =$ 0.10 rad (tuned for stair ascent) and $k_{spring} =$ 403 Nm/rad, $\theta_o = 0.00$ rad (tuned for walking).

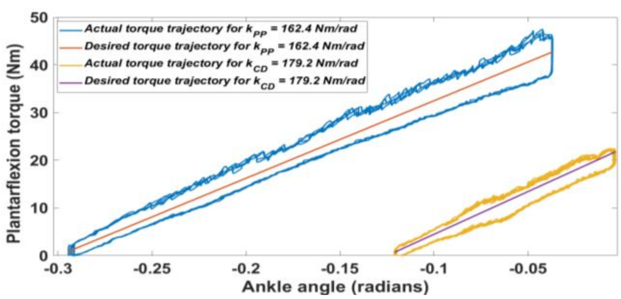

Figure 8. Impedance control tests for k_{PP} = 162.4 Nm/rad (derived from powered plantarflexion for k_{spring} = 403 Nm/rad at $\theta_o = 0.00$ rad) and k_{CD} = 179.2 Nm/rad (derived from controlled dorsiflexion for k_{spring} = 403 Nm/rad at $\theta_o = 0.00$ rad) for a feedback gain $k_f = 2$. The sudden discontinuities at the curve peaks can be attributed to change in the direction of stiction with a reversal in motion direction.

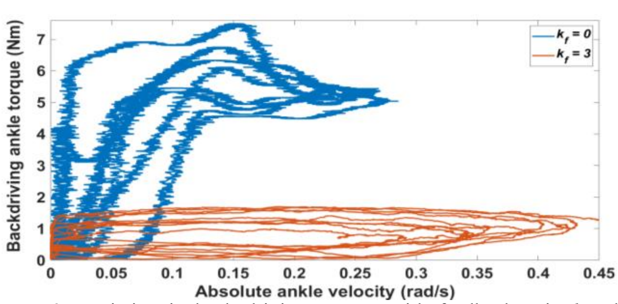

Figure 9. Variation in back driving torques with feedback gain k_f. The figure reveals the inherent device back drivability (back driving torque in the manually achievable range of 4.5-7.6 Nm) and an increase in device back drivability with an increase in feedback gain. The loops formed were caused by the system inertia.

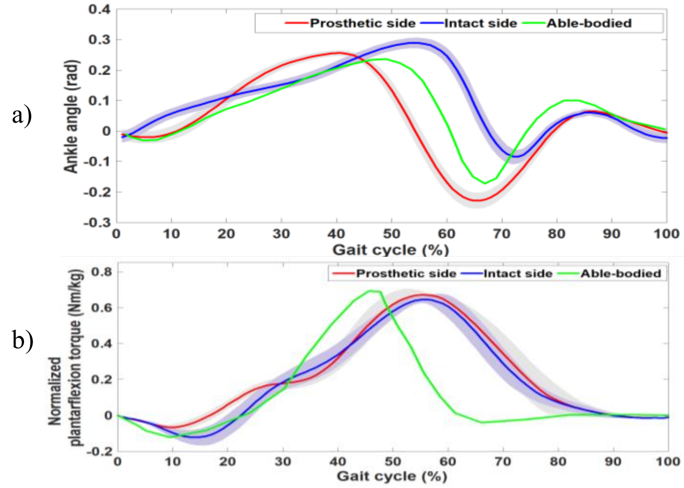

Figure 10. Comparison of (a) Ankle angle (rad) (b) Normalized Plantarflexion Torque for able-bodied individuals [28,29], the *VSeM* prosthesis, and the intact side. The solid red and blue lines represent the average over 16 steps. The grey and blue shaded portions represent one standard deviation for the prosthetic and intact side, respectively.

IV. Discussion and Future Scope

The *VSeM Ankle* prosthesis demonstrated promising performance and satisfied the design objectives. Even without the parallel elastic elements, the device can reach a peak torque of 138 Nm. Further improvement of the torque capability can be achieved using parallel elastic elements.

Despite its high torque capability, the *VSeM* ankle maintains a relatively low profile with 1.9 kg weight (without electronics) and 22cm height (foot cover included). At the same time, the ankle remained backdrivable as shown in Figure. 10. Its backdrivability was further improved through the implementation of force feedback. The capability of the *VSeM* to mimic targeted impedance and to support locomotion tasks are demonstrated in Fig. 8-11.

By adjusting the stack configurations, it can reach a ROM of 0.96 rad (-0.44 rad ~ 0.52rad) without the elastic element, a ROM of 0.70 rad (-0.44 rad ~ 0.19 rad) when stiffness of the elastic element was set at 403 Nm/rad at $\theta_o = 0.00$ rad, and a ROM of 0.80 rad (-0.44 rad ~ 0.36 rad), when the stiffness of the elastic element was set at 227 Nm/rad at $\theta_o = 0.10$ rad. The impact of the expanded ROM was demonstrated in the stair ascent test shown in Figure 12. The latter configuration (k_{spring} = 227 Nm/rad, $\theta_o = 0.10$ rad)

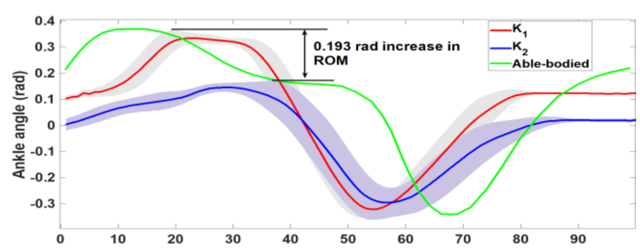

Figure 11. Comparison of Ankle angle trajectory during the stair ascent case for the prosthesis side with 2 different stack configurations where K_1 is k_{spring} = 227Nm/rad (red) with $\theta_0 = 0.10$ rad and K_2 is k_{spring} = 403Nm/rad (red) with $\theta_0 = 0.00$ rad, with that of an able-bodied individual [30]. The solid red and blue lines represent the average over 16 steps. The shadows show the standard deviation. The change of spring configuration expanded the ROM in dorsiflexion by about 0.193 rad.

better matches the ROM of an able-bodied individual compared to k_{spring} = 403 Nm/rad, θ_o = 0.00 rad (which was tuned for walking). By permitting quick adjustment of the dynamical properties (spring stiffness and equilibrium angle), this testing platform can be used to understand the potential of below knee amputees using powered prosthetic ankle while performing different locomotion tasks. Currently, these studies are often limited by the prosthetic leg's dynamical properties, which are often fixed.

Because the *VSeM* was developed for a research platform, it is optimized for high torque, which permits it to be evaluated in different locomotion tasks. Although flexible, the manual adjustment of the elastic elements leaves scope for improvement in the usability of the device, and a simple mechanism is under development to allow online automatic adjustment of the elastic elements. To avoid a high profile, the automatic adjustment will have no more than three configurations, which requires optimization of the elastic elements' properties, so they can support all the potential locomotion tasks without losing its efficiency and ROM. The performance of the human-prosthesis system was also hindered by the subject's very limited experience on prosthetic gait.

ACKNOWLEDGMENT

The authors would like to thank Dr. Xikai Tu, Albert Dodson, Steve Cameron, and Vince Chicarelli for their support in this work.

REFERENCES

[1] K. Hagberg & R. Brånemark (2001) Consequences of non-vascular trans-femoral amputation: A survey of quality of life, prosthetic use and problems, Prosthetics and Orthotics International, 25:3, 186-194.

[2] Legro MW, Reiber G, del Aguila M, Ajax MJ, Boone DA, Larsen JA, Smith DG, Sangeorzan B. Issues of importance reported by persons with lower limb amputations and prostheses. J Rehabil Res Dev. 1999 Jul;36(3):155-63.

[3] Zidarov D, Swaine B, Gauthier-Gagnon C. Quality of life of persons with lower-limb amputation during rehabilitation and at 3-month follow-up. Arch Phys Med Rehabil. 2009 Apr;90(4):634-45.

[4] Ziegler-Graham K, MacKenzie EJ, Ephraim PL, Travison TG, Brookmeyer R. Estimating the prevalence of limb loss in the United States: 2005 to 2050. Arch Phys Med Rehabil. 2008 Mar;89(3):422-9.

[5] H. Zhu, J. Doan, C. Stence, G. Lv, T. Elery and R. Gregg, "Design and validation of a torque dense, highly backdrivable powered knee-ankle orthosis," *2017 IEEE International Conference on Robotics and Automation (ICRA)*, 2017, pp. 504-510.

[6] S. K. Au, J. Weber and H. Herr, "Biomechanical Design of a Powered Ankle-Foot Prosthesis," *2007 IEEE 10th International Conference on Rehabilitation Robotics*, 2007, pp. 298-303.

[7] Gao, F., Liu, Y., and Liao, W. (March 9, 2018). "Design of Powered Ankle-Foot Prosthesis With Nonlinear Parallel Spring Mechanism." ASME. *J. Mech. Des*. May 2018; 140(5): 055001.

[8] Au S, Berniker M, Herr H. Powered ankle-foot prosthesis to assist level-ground and stair-descent gaits. Neural Netw. 2008 May;21(4):654-66.

[9] A. F. Azocar, L. M. Mooney, L. J. Hargrove and E. J. Rouse, "Design and Characterization of an Open-Source Robotic Leg Prosthesis," 2018 7th IEEE International Conference on Biomedical Robotics and Biomechatronics (Biorob), 2018, pp. 111-118.

[10] Lenzi T, Cempini M, Newkirk J, Hargrove LJ, Kuiken TA. A lightweight robotic ankle prosthesis with non-backdrivable cam-based transmission. IEEE Int Conf Rehabil Robot. 2017 Jul;2017:1142-1147.

[11] Shultz AH, Lawson BE, Goldfarb M. Variable Cadence Walking and Ground Adaptive Standing With a Powered Ankle Prosthesis. IEEE Trans Neural Syst Rehabil Eng. 2016 Apr;24(4):495-505.

[12] L. Gabert, S. Hood, M. Tran, M. Cempini and T. Lenzi, "A Compact, Lightweight Robotic Ankle-Foot Prosthesis: Featuring a Powered Polycentric Design," in IEEE Robotics & Automation Magazine, vol. 27, no. 1, pp. 87-102, March 2020.

[13] R. D. Bellman, M. A. Holgate and T. G. Sugar, "SPARKy 3: Design of an active robotic ankle prosthesis with two actuated degrees of freedom using regenerative kinetics," 2008 2nd IEEE RAS & EMBS International Conference on Biomedical Robotics and Biomechatronics, 2008, pp. 511-516.

[14] Hitt, JK, Bellman, R, Holgate, M, Sugar, TG, & Hollander, KW. "The SPARKy (Spring Ankle With Regenerative Kinetics) Project: Design and Analysis of a Robotic Transtibial Prosthesis With Regenerative Kinetics." *Proceedings of the ASME 2007 International Design Engineering Technical Conferences and Computers and Information in Engineering Conference. Volume 5: 6th International Conference on Multibody Systems, Nonlinear Dynamics, and Control, Parts A, B, and C*. Las Vegas, Nevada, USA. September 4–7, 2007. pp. 1587-1596. ASME.

[15] Winter, D. A. *The biomechanics and motor control of human gait*. (University of Waterloo Press, 1987).

[16] Protopapadaki A, Drechsler WI, Cramp MC, Coutts FJ, Scott OM. Hip, knee, ankle kinematics and kinetics during stair ascent and descent in healthy young individuals. Clin Biomech (Bristol, Avon). 2007 Feb;22(2):203-10.

[17] Lee JH, Chun MH, Jang DH, Ahn JS, Yoo JY. A comparison of young and old using three-dimensional motion analyses of gait, sit-to-stand and upper extremity performance. Aging Clin Exp Res. 2007 Dec;19(6):451-6.

[18] Fleming, A., Huang, S., Buxton, E., Hodges, F., & Huang, H. (2021). Direct continuous electromyographic control of a powered prosthetic ankle for improved postural control after guided physical training: A case study. *Wearable Technologies, 2021.*

[19] Glanzer EM, Adamczyk PG. Design and Validation of a Semi-Active Variable Stiffness Foot Prosthesis. IEEE Trans Neural Syst Rehabil Eng. 2018 Dec;26(12):2351-2359.

[20] M. K. Shepherd and E. J. Rouse, "The VSPA Foot: A Quasi-Passive Ankle-Foot Prosthesis With Continuously Variable Stiffness," in IEEE Transactions on Neural Systems and Rehabilitation Engineering, vol. 25, no. 12, pp. 2375-2386, Dec. 2017.

[21] M. E. Carney, T. Shu, R. Stolyarov, J. -F. Duval and H. Herr, "Design and Preliminary Results of a Reaction Force Series Elastic Actuator for Bionic Knee and Ankle Prostheses," in IEEE Transactions on Medical Robotics and Bionics.

[22] Bryan GM, Franks PW, Klein SC, Peuchen RJ, Collins SH. A hip–knee–ankle exoskeleton emulator for studying gait assistance. The International Journal of Robotics Research. 2021;40(4-5):722-746.

[23] Huang S, Wensman JP, Ferris DP. Locomotor Adaptation by Transtibial Amputees Walking With an Experimental Powered Prosthesis Under Continuous Myoelectric Control. IEEE Trans Neural Syst Rehabil Eng. 2016 May;24(5):573-81.

[24] Gates Corporation (2010) ,'Timing Belt Replacement Interval Guide', Edition:2010, Catalog 431-1448A

[25] C. Ott, A. Albu-Schaffer, A. Kugi, S. Stamigioli and G. Hirzinger, "A passivity based Cartesian impedance controller for flexible joint robots - part I: torque feedback and gravity compensation," IEEE International Conference on Robotics and Automation, 2004. Proceedings. ICRA '04. 2004, 2004, pp. 2659-2665 Vol.3.

[26] S. Culver, H. Bartlett, A. Shultz and M. Goldfarb, "A Stair Ascent and Descent Controller for a Powered Ankle Prosthesis," in *IEEE Transactions on Neural Systems and Rehabilitation Engineering*, vol. 26, no. 5, pp. 993-1002, May 2018.

[27] Vicon Motions Systems Ltd.,"Plug-in gait Reference Guide – lower body Modelling" Pg. 6-17.

[28] Mentiplay BF, Banky M, Clark RA, Kahn MB, Williams G. Lower limb angular velocity during walking at various speeds. Gait Posture. 2018 Sep;65:190-196.

[29] Lencioni, T., Carpinella, I., Rabuffetti, M. *et al.* Human kinematic, kinetic and EMG data during different walking and stair ascending and descending tasks. *Sci Data* **6,** 309 (2019).

[30] Sinitski EH, Hansen AH, Wilken JM. Biomechanics of the ankle-foot system during stair ambulation: implications for design of advanced ankle-foot prostheses. J Biomech. 2012 Feb 2;45(3):588-94.